Motional Impedance Analysis: Bridging the 'Gap' in Dielectric Transduction

Siddharth Tallur, Tiffany J. Cheng, Suresh Sridaran, Sunil A. Bhave
OxideMEMS Laboratory, Cornell University
Ithaca, NY USA

Abstract — **This paper presents an analytical model to estimate the motional resistance for partial air gap capacitively-transduced MEMS resonators. This model serves as a link between the well formulated analytical models for conventional air gap and internal dielectric transduction schemes, thereby helping decide which scheme is optimal for a given design frequency. Using this model, we simulate and experimentally verify the motional resistance for a 303MHz polysilicon disk resonator within a 5% range of accuracy.**

I. Introduction

Semiconductor electromechanical resonators, with quality factors (Q) often >10000, provide a low-power small-footprint CMOS-compatible alternative to various electrical components in wireless communication and signal processing. On-chip fabrication of high Q micromechanical resonators can enable low-cost, miniature, low-power filter banks for radio front ends. Moreover, such resonators have promising applications in high performance microprocessors for synchronized clocking arrays with low power, jitter and skew.

Conventional air gap capacitively-transduced RF MEMS resonators typically have high motional impedances on the order of a few kΩ [1, 2]. Sub-GHz partial gap resonators with 10 nanometer air gaps achieving impedances <1kΩ have been shown [3, 4]. Extending the frequency of these resonators entails scaling of resonator dimensions, leading to increased motional impedance at higher frequencies. Dielectric electrostatic transduction has several benefits over conventional capacitive air gap transduction schemes for higher frequencies and smaller dimensions [5]. However, there is no clear understanding on which of these transduction schemes is better for a given design frequency and desired mode shape of the resonator. This work presents an analytical treatment of this problem, and insights derived from the equations presented here enable the designer to optimize resonator designs for low motional impedances.

Primary contact: Siddharth Tallur, sgt28@cornell.edu

II. Prior Modeling efforts

Motional impedance models for air gap transducers [6] and internal dielectric transduced resonators [5] are available in literature. However, partial air gap transduction lacks a good analytical Butterworth Van-Dyke (BVD) model in literature that can accurately predict resonator performance for varied applications. Designers often feel the need for a complete model for dielectric transduction that can help them determine the motional impedance for various schemes for their design of choice, thereby enabling them to pick a scheme that works best. An earlier attempt to model partial gap beam resonators [3] was limited by distortions of the beam geometry at the resonator-electrode interface, resulting in significant deviation from measured results. The next section presents a model that is built on the methodology presented in [6]. However, there are many additional factors to be considered for the case of partial air gap transduced resonators, such as motion of the dielectric, acoustic mismatch between the dielectric and resonator body, stress in the resonator etc. For this simple zero-order model we have made several assumptions that are listed in the following section.

III. Assumptions and methodology

A. Assumptions

The model presented here makes several assumptions to simplify the derivation. Consider a schematic of a beam resonator shown in fig. 1 for illustration. The resonator body comprises of a resonator body of length L and dielectric of length d_2 at both ends. The air gap is d_1 and the dielectric on the electrode has length d_e. The dielectric constant of the dielectric is ε_2 and that of air is ε_1. The various assumptions made are:

1. No acoustic mismatch between dielectric and resonator body.
2. Dielectric on the electrode is rigid.
3. Expressions for electrostatic forces are independent of the mode shape
4. Sense current calculation requires:
   - 4.1. Accounting for both displacement in x (motion at the free end) and displacement in y (motion at the interface between resonator and dielectric).
   - 4.2. Expressing x displacement in terms of y displacement.

978-1-61284-110-6/11/$26.00 ©2011 IEEE

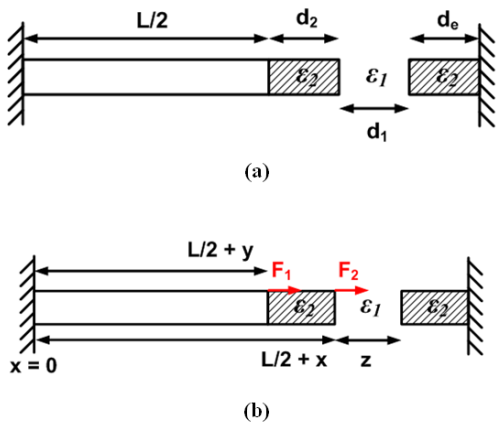

Fig 1. Schematic highlighting half the resonator geometry for a beam resonator for illustrating model assumptions and methodology

B. Methodology

The model essentially follows the derivation for motional impedance presented in [6]. As listed in step 4-5 below, we need to account for motion at the resonator-dielectric interface and air-dielectric interface also.

1. Write down the equation for mode shape in the resonator assuming no acoustic mismatch.
2. Express total capacitance between electrode and resonator body (dielectric and air gap combination) in terms of displacements.
3. Express forces in the form $F_i = \frac{V^2}{2}\frac{\partial C_{tot}}{\partial x_i}$ where V is the total applied voltage, C_{tot} is the total capacitance and x_i is the corresponding displacement.
4. Write down displacement amplitude, and hence the velocity amplitude at the free end of the resonator in terms of effective force (sum of individual forces shaped by the mode shape), stiffness and the quality factor.
5. Use these expressions to write down sense current as $i_{sense} = V_{dc}\frac{dC_{tot}}{dgap} = V_{dc}\frac{\partial C_{tot}}{\partial gap}\frac{\partial gap}{\partial t}$, where V_{dc} is the DC bias applied across the resonator.
6. Express the motional resistance R_x in terms of the applied RF voltage v_{ac} as $R_x = \frac{v_{ac}}{i_{sense}}$
7. Comparing the expression for effective force from step 4 with $F_{net} = \eta v_{ac}$, find the effective electromechanical transduction factor η.
8. Expressions for the inductance and capacitance are given by $L_x = \frac{M}{\eta^2}, C_x = \frac{\eta^2}{K}$, where M is the effective mass and K is the stiffness.

C. Equations for a beam resonator

The equations for a beam resonator can be obtained by following the methodology presented in sub-section B. For the schematic presented in fig. 1, the mode shape can be written as in equation (1), where U_0 is the amplitude of displacement, $k_n = \frac{(2n+1)\pi}{(L+2d_2)}$ is the wave number and ω is the frequency.

$$u(x) = U_0 \sin(k_n x) e^{j\omega t} \tag{1}$$

The total capacitance, C_{tot} can be written as

$$C_{tot} = \frac{\varepsilon_2\varepsilon_1 A}{\varepsilon_1 d_e + \varepsilon_2(d_1+d_2) + x(\varepsilon_1-\varepsilon_2) - \varepsilon_1 y} \tag{2}$$

The forces at resonator-dielectric and air-dielectric interfaces can be written as follows, where V is the voltage applied at the electrode. For our purposes we use expressions obtained by substituting x = d_2 and y = 0. Moreover, we have $\frac{V^2}{2} = V_{dc} v_{ac}$

$$F_1 = \frac{V^2}{2}\frac{\partial C_{tot}}{\partial y} = \frac{V^2}{2}\frac{\varepsilon_2\varepsilon_1^2 A}{[\varepsilon_1 d_e + \varepsilon_2(d_1+d_2) + x(\varepsilon_1-\varepsilon_2) - \varepsilon_1 y]^2} \tag{3}$$

$$F_2 = \frac{V^2}{2}\frac{\partial C_{tot}}{\partial x} = -\frac{V^2}{2}\frac{\varepsilon_2\varepsilon_1 A(\varepsilon_1-\varepsilon_2)}{[\varepsilon_1 d_e + \varepsilon_2(d_1+d_2) + x(\varepsilon_1-\varepsilon_2) - \varepsilon_1 y]^2} \tag{4}$$

$$F_{net} = F_1 \sin\left(\frac{k_n L}{2}\right) + F_2 \tag{5}$$

The expression for displacement can be written down as in equations (6)-(7) using expression for stiffness from [5].

$$U_0 = \frac{F}{|b\omega_0|} = \frac{F}{\left|\frac{m\omega_0^2}{Q}\right|} = \frac{FQ}{K} \tag{6}$$

$$\therefore U_0 = \frac{2Q(L+2d_2)}{Y(2n+1)^2\pi^2}\frac{\varepsilon_2\varepsilon_1 V_{dc} v_{ac}\left\{\varepsilon_1 \sin\left(\frac{k_n L}{2}\right) - (\varepsilon_1-\varepsilon_2)\right\}}{[\varepsilon_2 d_1 + \varepsilon_1 d_2 + \varepsilon_1 d_e]^2} \tag{7}$$

Then the sense current can be written as

$$i_{sense} = V_{dc}\frac{dC_{tot}}{dgap} = V_{dc}\frac{\partial C_{tot}}{\partial gap}\frac{\partial gap}{\partial t} = V_{dc}\frac{\partial C_{tot}}{\partial y}\frac{\partial y}{\partial t} \tag{8}$$

While carrying out this derivation, we express x in terms of y. The reason for this is that motion at the free end also contributes to the sense current which wouldn't be captured if we only carry out a partial differentiation of C_{tot} with y.

$$x = d_2 + \frac{y}{\sin\left(\frac{k_n L}{2}\right)}, \frac{\partial y}{\partial t} = 2\pi f_n U_0 \sin\left(\frac{k_n L}{2}\right) \tag{9}$$

Thus, we can get an expression for R_x as follows:

$$R_x = \frac{v_{ac}}{i_{sense}} = \frac{(2n+1)\pi\sqrt{Y\rho}}{2QV_{dc}^2\varepsilon_1^2\varepsilon_2^2 A}\frac{[\varepsilon_2 d_1+\varepsilon_1 d_2+\varepsilon_1 d_e]^4}{\left\{\varepsilon_1 \sin\left(\frac{k_n L}{2}\right)-(\varepsilon_1-\varepsilon_2)\right\}^2} \quad (10)$$

We obtain η from (5), and thus can express L_x and C_x as follows:

$$L_x = \frac{\rho(L+2d_2)[\varepsilon_2 d_1+\varepsilon_1 d_2+\varepsilon_1 d_e]^4}{\varepsilon_1^2\varepsilon_2^2 V_{dc}^2 A\left\{\varepsilon_1 \sin\left(\frac{k_n L}{2}\right)-(\varepsilon_1-\varepsilon_2)\right\}^2} \quad (11)$$

$$C_x = \frac{2\varepsilon_1^2\varepsilon_2^2 V_{dc}^2 A(L+2d_2)\left\{\varepsilon_1 \sin\left(\frac{k_n L}{2}\right)-(\varepsilon_1-\varepsilon_2)\right\}^2}{Y\pi^2(2n+1)^2[\varepsilon_2 d_1+\varepsilon_1 d_2+\varepsilon_1 d_e]^4} \quad (12)$$

D. Equations for a disk resonator

Beam resonators have significant mode distortion at the resonator-electrode interface [3] that are not accounted for in this model. However, we can establish the validity of this model by deriving a similar set of equations for disk resonators which do not have mode distortion.

Consider the disk resonator geometry in fig. 2. The mode shape for disk resonators can be written as [8] in (13) where $k_0 = \omega_0(R+d_2)\sqrt{\frac{\rho(1-\nu^2)}{E}}$

$$u(r) = A\frac{k_0}{R}J_1\left(\frac{k_0 r}{R}\right)e^{j\omega t} \quad (13)$$

The total capacitance can be written as follows:

$$C_{tot} = \frac{t}{\frac{1}{\theta\varepsilon_2}\ln\left(\frac{R+d_2+d_1+d_e}{R+d_2+d_1}\right)+\frac{1}{\theta\varepsilon_1}\ln\left(\frac{R+d_2+d_1}{R+d_2+x}\right)+\frac{1}{2\pi\varepsilon_2}\ln\left(\frac{R+d_2+x}{R+y}\right)} \quad (14)$$

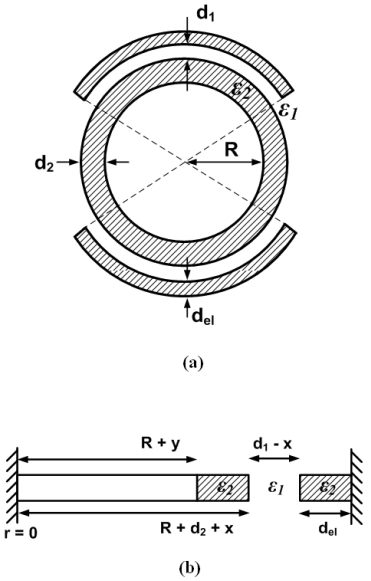

Fig 2. Schematic for a partial gap disk resonator highlighting (a) the geometry, (b) displacements at various interfaces

One can derive the stiffness (and hence effective mass) from the modeling presented in [8]

$$K = \pi\rho t(R+d_2)^2\omega_0^2\frac{J_2^2(k_0)}{J_1(k_0)} \quad (15)$$

Also, the forces and hence the effective force can be written down as in equations (16)-(18)

$$F_1|_{y=0,x=0} = \frac{V^2}{2}\frac{\partial C_{tot}}{\partial y} = V_{dc}v_{ac}\frac{\partial C_{tot}}{\partial y} \quad (16)$$

$$F_2|_{y=0,x=0} = \frac{V^2}{2}\frac{\partial C_{tot}}{\partial x} = V_{dc}v_{ac}\frac{\partial C_{tot}}{\partial x} \quad (17)$$

$$F_{net} = \frac{F_1 J_1\left(\frac{k_0 R}{R+d_2}\right)}{J_1(k_0)} + F_2 \quad (18)$$

The displacement amplitude can then be written down as follows:

$$U_0 = \frac{FQ}{K} = \frac{QV_{dc}v_{ac}\left[\frac{J_1\left(\frac{k_0 R}{R+d_2}\right)}{J_1(k_0)}\frac{\partial C_{tot}}{\partial y}+\frac{\partial C_{tot}}{\partial x}\right]_{x=0,y=0}}{\pi\rho t(R+d_2)^2\omega_0^2\frac{J_2^2(k_0)}{J_1(k_0)}} \quad (19)$$

Similar to (8)-(9), we obtain

$$i_{sense} = V_{dc}\frac{\partial C_{tot}}{\partial y}\frac{\partial y}{\partial t} \quad (20)$$

$$x = \frac{yJ_1(k_0)}{J_1\left(\frac{k_0 R}{R+d_2}\right)},\ \frac{dy}{dt} = \omega_0 U_0\frac{J_1\left(\frac{k_0 R}{R+d_2}\right)}{J_1(k_0)} \quad (21)$$

Thus we can obtain following expressions for R_x, L_x and C_x

$$R_x = \frac{\pi\rho t(R+d_2)^2\omega_0 J_2^2(k_0)}{QV_{dc}^2\left[\frac{J_1\left(\frac{k_0 R}{R+d_2}\right)}{J_1(k_0)}\frac{\partial C_{tot}}{\partial y}+\frac{\partial C_{tot}}{\partial x}\right]_{x=0,y=0}\left[\frac{dC_{tot}}{dy}\right]_{x=\frac{yJ_1(k_0)}{J_1\left(\frac{k_0 R}{R+d_2}\right)},y=0}J_1\left(\frac{k_0 R}{R+d_2}\right)} \quad (22)$$

$$L_x = \frac{\pi\rho t(R+d_2)^2 J_2^2(k_0)}{J_1(k_0)\left\{V_{dc}\left[\frac{J_1\left(\frac{k_0 R}{R+d_2}\right)}{J_1(k_0)}\frac{\partial C_{tot}}{\partial y}+\frac{\partial C_{tot}}{\partial x}\right]_{x=0,y=0}\right\}^2} \quad (23)$$

$$C_x = \frac{J_1(k_0)\left\{V_{dc}\left[\frac{J_1\left(\frac{k_0 R}{R+d_2}\right)}{J_1(k_0)}\frac{\partial C_{tot}}{\partial y}+\frac{\partial C_{tot}}{\partial x}\right]_{x=0,y=0}\right\}^2}{\omega_0^2\pi\rho t(R+d_2)^2 J_2^2(k_0)} \quad (24)$$

IV. DISCUSSIONS

We compare the model for a beam resonator in the limiting cases of air gap transduction and internal dielectric transduction. The equation for air gap transduction is

presented in (25) [6], and the equation derived from our model is presented in (26).

$$R_x = \frac{\sqrt{KM}}{Q\eta^2} = \frac{(2n+1)\pi d^4\sqrt{Y\rho}}{2QV_{dc}^2\varepsilon_0^2 A} \quad (25)$$

$$R_x = \frac{v_{ac}}{i_{sense}} = \frac{(2n+1)\pi d_1^4\sqrt{Y\rho}}{2QV_{dc}^2\varepsilon_1^2 A} \quad (26)$$

Similarly, equations (27) and (28) present equations for the fundamental mode for internal dielectric transduced resonators in literature [5] and from our model respectively.

$$R_x = \frac{\pi g^4\sqrt{Y\rho}}{2QV_{dc}^2\varepsilon_2^2 A\left\{\sin\left(\frac{k_0 L}{2}\right)\right\}^2} \quad (27)$$

$$R_x = \frac{\pi(d_2+d_e)^4\sqrt{Y\rho}}{2QV_{dc}^2\varepsilon_2^2 A\left\{\sin\left(\frac{k_0 L}{2}\right)\right\}^2} \quad (28)$$

The model converges to the well established models for both cases, thereby serving as a 'bridge' between them.

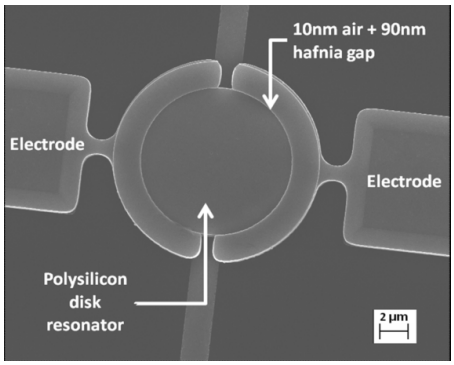

Fig 3. Scanning electron micrograph of the radial breathing mode disk resonator actuated through a 10nm air + 90nm hafnia gap fabricated as in [3]

TABLE I. COMPARISON OF PREDICTED RESISTANCE FROM MODEL TO MEASURED RESISTANCE FOR A WINE GLASS MODE DISK RESONATOR [7]

Process	*Measured R_x (Ω) [7]*	*Predicted R_x (Ω)*
a) 94nm air gap after HF release	2.62k	2.24k
b) After partially filling gap with 30.7nm HfO_2 and sintering at 400°C for 3 minutes	966	869
c) Same conditions as (b) with lower V_{DC}	6.5k	5.23k
d) After sintering at 400°C for another 3 minutes	685	516

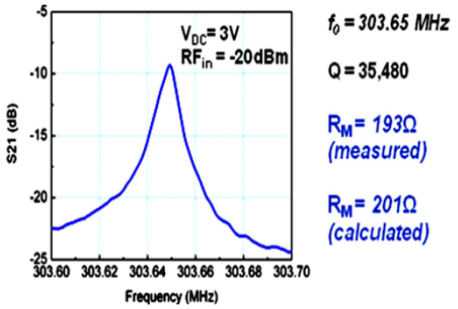

Fig 4. Transmission response of the resonator shown in fig. 3 highlighting measured resistance value

V. COMPARISON OF MODEL TO MEASURED RESULTS

We compared predictions made from our model to measured motional resistance for a radial breathing mode disk resonator designed at OxideMEMS laboratory. The resonator comprises of a poly silicon disk resonator with a radius of 8.83µm actuated through a 10nm air + 90nm hafnia gap. Fig. 3 shows a scanning electron micrograph of this resonator. As shown in the transmission response of the resonator in fig. 4, the predicted motional resistance from the model matches the measured resistance value to within 5% accuracy. To further corroborate the validity of the model, we compared predictions from the model to a wine-glass mode disk resonator reported earlier [7] in table 1.

The model thus compares quite well for measured resistance for these disk resonator geometries. For higher accuracy, the model must include the effects of strain in the dielectric and acoustic mismatch [9] to make it useful for varied applications [10] of partial air gap transduced resonators.

ACKNOWLEDGMENT

The authors extend their thanks to Prof. Ehsan Afshari at Cornell University for interesting discussions on modeling electrostatic forces and NSF career award for support.

REFERENCES

[1] S. Pourkamali, G.K. Ho, F. Ayazi, *IEEE Transactions on Electron Devices,* vol.54, no.8, pp.2024-2030.

[2] Y.-W. Lin, S.-S. Li, Z. Ren, C.T.-C. Nguyen, *Tech. Digest IEDM 2005*, pp. 278-281.

[3] T. Cheng and S.A. Bhave, *Proc. MEMS 2010,* pp. 695-698..

[4] M. Akgul, B. Kim, Z. Ren, C.T.-C. Nguyen, *Hilton Head, SC*, pp.467-470, June 6-10, 2010.

[5] D. Weinstein and S.A. Bhave, *J. Microelectromech. Syst.*, 18.6, pp. 1401-1408, 2009.

[6] V. Kaajakari, A.T. Alastalo, T. Mattila, *IEEE Transactions on UFFC,* 53 (12), pp. 2484-89, 2006.

[7] L.-W. Hung, Z.A. Jacobson, Z. Ren, A. Javey, C.T.-C. Nguyen, *Hilton Head, SC*, pp.208-211, June 1-5, 2008.

[8] Z. Hao, S. Pourkamali, F. Ayazi , *IEEE J. Microelectromech. Syst.* 13, pp. 1054–1062, 2004

[9] E. Hwang, S.A. Bhave, *IEEE Transactions on Ultrasonics, Ferroelectrics, and Frequency Control,* 57(7), pp. 1664-1672, 2010.

[10] R. Melamud, B. Kim, M. Hopcroft, S. Chandorkar, M. Agarwal, C. Jha, and T. Kenny, *Proc. IEEE Int. Conf.MEMS, Kobe, Japan, 2007*, pp. 199–202.